Abdelatif, Amged O. and Owen, John S. and Hussein, Mohammed F.M. (2012) Modeling the re-anchoring of a ruptured tendon in bonded post-tensioned concrete. In: Bond in Concrete 2012 – General Aspects of Bond, 2012, Italy.

Modeling the Re-anchoring of a Ruptured Tendon in Bonded Post-tensioned Concrete

A.O. Abdelatif , J.S. Owen , M.F.M. Hussein
University of Nottingham, Nottingham, UK

ABSTRACT: In this study, a theoretical model is developed to simulate the re-anchorage of a ruptured bonded post-tensioning tendon. This includes estimating the re-anchorage length and stress distribution over the tendon. The model accounts for equilibrium and compatibility conditions at the steel-grout, grout-duct and duct-concrete interfaces as well as the effect of axial stresses in the strand and its confining materials, i.e. grout, duct and concrete. Formulation of the model is based on the elastic theory of thick-wall cylinders and the Coulomb friction model. The model has been validated against an axi-symmetrical Finite Element (FE) model, the UK Highway Agency's BA51/95 model and previous experimental data. The models had been compared with the UK Highway Agency's BA51/95 model and previous experimental data.

1 INTRODUCTION

Post-tensioned concrete has proven to be a durable and economical form of construction. However, many bonded post-tensioned concrete bridges have been reported to have ruptured tendons due to corrosion (Concrete Society 2002, Great Britain Highways Agency et al., 1999, NCHRP, 1998). In some extreme cases this led to a structural collapse (Woodward and Williams, 1989, Concrete Society 2002). While much of the effort has been focused on developing corrosion detection techniques, little attention has been paid to assessing the structural capacity of bonded post-tensioned concrete structures with ruptured tendon. A ruptured tendon is able to re-anchor into the surrounding grout, which is mainly designed as a corrosion protection, and, as a result, contributes to the residual structural capacity of the structure (Highway Agency, 1995, Buchner and Lindsell, 1987). This is because of activation of the bond between grout and post-tensioning steel after rupture.

A number of structural assessment studies used pre-tensioned models or empirical bond slip relations to approximately estimate the re-anchorage length (Cavell and Waldron, 2001, Coronelli et al., 2009). In some cases, re-anchoring of ruptured tendon is completely neglected (Jeyasehar and Sumangala, 2006, Zeng et al., 2010, Watanabe et al., 2011). This is attributed to the lack of models regarding the re-anchorage phenomenon of the ruptured tendon in post-tensioned concrete beams. Wrong estimation of re-anchoring phenomenon of the ruptured tendon influences the prediction of structural behavior of post-tensioned concrete beams. Therefore it is important to develop a model to describe re-anchoring of ruptured tendon. The model will facilitate the understanding of the behavior of post-tensioned concrete beams having ruptured tendons as well as the prediction of their residual structural capacity.

2 BOND IN GROUTED POST-TENSIONED CONCRETE ELEMENTS

The bond between steel and grout is attributed to three factors: adhesion between steel and grout, friction between steel and grout, and mechanical resistance. The adhesion is the chemical and physical reaction between cement paste and steel surface. It always has insignificant influence on load-deformation response because the adhesion fails after very small relative slip (Marti et al., 2008). The mechanical resistance only contributes in bond when deformed steel is used. So, the dry friction between steel and grout is largely responsible for the transfer of stress into the surrounding materials.

Geddes and Soroka tested 19 beams to study the effect of the grout properties on the transmission length and to investigate the structural behavior of bonded post-tensioned concrete beams (Geddes and Soroka, 1963, Geddes and Soroka, 1964). Their results showed that the transmission length is independent of time, and it is affected by the compressive strength of the grout.

(Schupack and Johnston, 1974) carried out a series of tests to find out the bond development length

of a grouted 54 strand post-tensioned tendon in curved duct.

The controlled demolition of Taf Fawar Bridge and monitoring of Basingstoke, Orpington and Abercynon bridges were reported in (Buchner and Lindsell, 1987) and (Buchner and Lindsell, 1988) respectively. The results revealed important information about the damage that might be caused to a structure suffering from corrosion. It was found that the ruptured tendon is able to re-anchor into surrounding material over a certain length known as the re-anchorage length. The re-anchoring of a ruptured tendon was found to depend on grout condition, friction between individual wires or strand within a tendon, and the level of confinement provided by shear links.

Euro-International Committee for Concrete (CEB) and International Federation for Pre-stressing (FIP) introduced a model of bond between concrete and the tendons the outer surface of sheathing (CEB-FIP MC90, 1990). In reality the bond actually occurs between steel and grout rather than between steel and concrete.

The UK Highway Agency proposed an empirical relation to estimate re-anchorage length conservatively (Highway Agency, 1995). The relation modified the (BS 5400 - 4, 1990) transfer length model for pre-tensioned concrete element to account for multi-strand tendons. The model assumes linear distribution of tendons stresses over the re-anchorage length.

$$l_t = \frac{k_t D}{\sqrt{f_{ci}}} * \sqrt{S} \qquad (1)$$

(Belhadj and Bahai, 2001) performed a Finite Element model and experimental investigation to study the movement of smooth pre-stressing bar embedded in grout. The study demonstrated the importance of friction in controlling the slip of pre-stressing steel in grout.

(Marti et al., 2008, Luthi et al., 2008) investigated the effect of emulsfiable oils, which is used as a temporary corrosion protection, and the types of ducts on the bond behavior of the bonded post-tensioned tendon.

All the reviewed literature addressing the bond of post-tensioned tendon had aimed to study the influence of some parameters on the bond mechanism rather than developing a model for bond. Therefore the aim of this study is to propose a model that describes the re-anchoring of ruptured bonded tendon in post-tensioned concrete elements. This paper presents a theoretical model simulating the re-anchoring phenomenon. The model is 2D with linear materials properties. The results of the models were compared to previous experimental data and DMRB - BA 51/95 model (Highway Agency, 1995).

3 THEORETICAL MODELLING OF THE BOND OF RUPTURED POST-TENSIONED TENDON

The transfer of force from ruptured tendon/s to the post-tensioned concrete units follows the same behavior as in pre-tensioned concrete elements. The only difference is that the post-tensioning steel is surrounded by grout, duct and concrete.

When the tendon is ruptured, the tendon's section at the rupturing point tries to return to the original diameter, whilst within the re-anchorage length, the tendon diameter varies as a result of Poisson's effect forming a wedge shape (Janney, 1954). The increase in the diameter exerts a radial pressure onto surrounding materials (i.e. grout, duct, and concrete). The exerted pressure produces a frictional component which helps in transferring the force in the ruptured tendon gradually into the surrounding material over the re-anchorage length. This action is known as wedge action or Hoyer effect (Gilbert and Mickleborough, 1990), it enhances the possibility of re-anchorage of the ruptured tendon and thus the structural capacity of the post-tensioned concrete element.

To find out the distribution of forces along the ruptured tendon, the compatibility conditions and equilibrium of forces need to be satisfied at each interface, i.e. the interface between pre-stressing steel and grout, the interface between grout and duct and the interface between duct and concrete.

3.1 Compatibility conditions

Compatibility conditions can be satisfied by examining the radial deformation at each interface. Radial deformations are calculated by considering the post-tensioning steel as a solid cylinder confined by a hollow grout cylinder with uniform thickness, both of them are surrounded by a duct and hollow concrete cylinder with external radius equal to concrete cover, (Figure 1), (Janney, 1954).

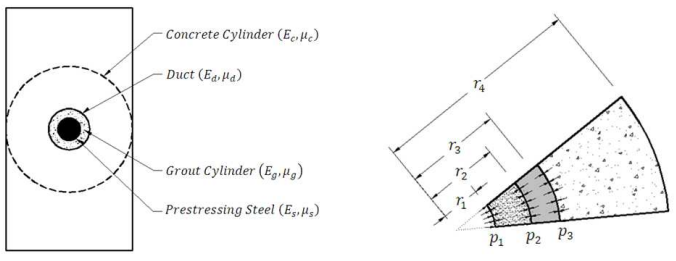

Figure 1: Post-tensioned cylinders and interfaces

The radial deformation of hollow cylinder subjected to the internal, external and longitudinal stresses can be expressed as follow based on the thick-wall cylinder theory, (Figure 2), (Timoshenko, 1976):

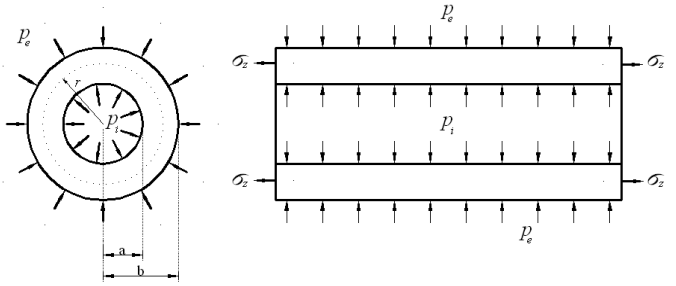

Figure 2: Hollow cylinder

$$u_r = \left[\frac{1-\mu}{E}\frac{a^2 p_i - b^2 p_e}{\left(b^2-a^2\right)} - \frac{\mu\sigma_z}{E}\right] r + \left[\frac{1+\mu}{E}\frac{a^2 b^2 \left(p_i - p_e\right)}{\left(b^2-a^2\right)}\right]\frac{1}{r} \tag{2}$$

Compatibility at interface 1: Between pre-stressing steel and the grout

At the interface between the pre-stressing steel and grout, the two cylinders must satisfy the compatibility condition, that is, the outer perimeter of steel must be equal to the inner perimeter of hollow grout cylinder after the radial deformation.

$$r_s + u_{r,s_1} = r_{g_1} + u_{r,g_1} \tag{3}$$

Radial deformation of the outer diameter of post-tensioned bar can be get as follow:

$$u_{r,s_1} = \frac{-p_1\left(1-\mu_s\right)}{E_s} r_s - \frac{\mu_s f_s}{E_s} r_s \tag{4}$$

Inner diameter of the grout cylinder deformed by:

$$u_{r,g_1} = \left[\frac{1-\mu_g}{E_g}\frac{r_{g_1}{}^2 p_1 - r_{g_2}{}^2 p_2}{\left(r_{g_2}{}^2 - r_{g_1}{}^2\right)} - \frac{-f_g\mu_g}{E_g}\right] r_{g_1} + \left[\frac{1+\mu_g}{E_g}\frac{r_{g_1}{}^2 r_{g_2}{}^2\left(p_1-p_2\right)}{\left(r_{g_2}{}^2 - r_{g_1}{}^2\right)}\right]\frac{1}{r_{g_1}} \tag{5}$$

Stress at any section in grout, duct, and concrete can be given by assuming uniform distribution as follows:

$$f_g = f_d = f_c = \frac{f_s A_s}{A_b} \tag{6}$$

where:

$$A_b = A_g + A_d + A_c$$

Substituting deformations of steel radius and grout's inner radius in the compatibility equation of interface between the two materials gives:

$$r_s + \frac{-p_1\left(1-\mu_s\right)}{E_s} r_s - \frac{\mu_s f_s}{E_s} r_s = r_{g_1} + \left[\frac{1-\mu_g}{E_g}\frac{r_{g_1}{}^2 p_1 - r_{g_2}{}^2 p_2}{\left(r_{g_2}{}^2 - r_{g_1}{}^2\right)} - \frac{-f_g\mu_g}{E_g}\right] r_{g_1} + \left[\frac{1+\mu_g}{E_g}\frac{r_{g_1}{}^2 r_{g_2}{}^2\left(p_1-p_2\right)}{\left(r_{g_2}{}^2 - r_{g_1}{}^2\right)}\right]\frac{1}{r_{g_1}} \tag{7}$$

For simplification equation (7) can be written in form of:

$$C_1 p_1 + C_2 p_2 + C_3 p_3 + K_1 = 0 \tag{8}$$

Compatibility at interface 2: Between Grout and duct

Here the outer radius of grout cylinder should equal the inner radius of the duct after deformation.

$$r_{g_2} + u_{r,g_2} = r_{d_2} + u_{r,d_2} \tag{9}$$

Substituting radial deformations (from equation (2)) into the compatibility equation yields:

$$r_{g_2} + \left[\frac{1-\mu_g}{E_g}\frac{r_{g_1}{}^2 p_1 - r_{g_2}{}^2 p_2}{\left(r_{g_2}{}^2 - r_{g_1}{}^2\right)} - \frac{-f_g\mu_g}{E_g}\right] r_{g_2} + \left[\frac{1+\mu_g}{E_g}\frac{r_{g_1}{}^2 r_{g_2}{}^2\left(p_1-p_2\right)}{\left(r_{g_2}{}^2 - r_{g_1}{}^2\right)}\right]\frac{1}{r_{g_2}} = r_{d_2} + \left[\frac{1-\mu_d}{E_d}\frac{r_{d_2}{}^2 p_2 - r_{d_3}{}^2 p_3}{\left(r_{d_3}{}^2 - r_{d_2}{}^2\right)} - \frac{-f_d\mu_d}{E_d}\right] r_{d_2} + \left[\frac{1+\mu_d}{E_d}\frac{r_{d_2}{}^2 r_{d_3}{}^2\left(p_2-p_3\right)}{\left(r_{d_3}{}^2 - r_{d_2}{}^2\right)}\right]\frac{1}{r_{d_2}} \tag{10}$$

By substitution of stresses in grout and duct using equation (6), equation (10) can be rewritten as:

$$C_4 p_1 + C_5 p_2 + C_6 p_3 + K_2 = 0 \tag{11}$$

Compatibility at interface 3: Between duct and concrete

The duct outer radius must be equal to the inner radius of the concrete cylinder after the deformation.

$$r_{d_3} + u_{r,d_3} = r_{c_3} + u_{r,c_3} \tag{12}$$

Substitution of deformations at the interface (i.e. u_{r,d_3} and u_{r,c_3}), the compatibility equation gives:

$$r_{d_3}+\left[\frac{1-\mu_d}{E_d}\frac{r_{d_2}{}^2 p_2-r_{d_3}{}^2 p_3}{\left(r_{d_3}{}^2-r_{d_2}{}^2\right)}-\frac{-f_d\mu_d}{E_d}\right]r_{d_3}+\left[\frac{1+\mu_d}{E_d}\frac{r_{d_2}{}^2 r_{d_3}{}^2\left(p_2-p_3\right)}{\left(r_{d_3}{}^2-r_{d_2}{}^2\right)}\right]\frac{1}{r_{d_3}}=$$
$$r_{c_3}+\left[\frac{1-\mu_c}{E_c}\frac{r_{c_3}{}^2 p_3}{\left(r_{c_4}{}^2-r_{c_3}{}^2\right)}-\frac{-f_c\mu_c}{E_c}\right]r_{c_3}+\left[\frac{1+\mu_c}{E_c}\frac{r_{c_3}{}^2 r_{c_4}{}^2 p_3}{\left(r_{c_4}{}^2-r_{c_3}{}^2\right)}\right]\frac{1}{r_{c_3}} \quad (13)$$

This equation can be expressed as follows:

$$C_7 p_1+C_8 p_2+C_9 p_3+K_3=0 \quad (14)$$

Equations of compatibility at each interface can be written in matrix form:

$$\begin{bmatrix}C_1 & C_2 & C_3\\ C_4 & C_5 & C_6\\ C_7 & C_8 & C_9\end{bmatrix}\begin{bmatrix}p_1\\ p_2\\ p_3\end{bmatrix}+\begin{bmatrix}k_1\\ k_2\\ k_3\end{bmatrix}=0 \quad (15)$$

Solving the compatibility equation (15) gives the magnitude of radial pressures p_1, p_2 and p_3. p_1 can be written in the following form:

$$p_1=A+Bf_s \quad (16)$$

Where: A and B are coefficients that depend on both physical and geometrical properties of the components of the post-tensioned concrete element, (i.e. concrete, duct, grout and post-tensioning steel).

3.2 Equilibrium conditions

Difference in stresses at ends of a definite element dx of pre-stressing steel in the re-anchoring zone develops a tensile force. The frictional bond force resists the slippage caused by the tensile force as shown below in Figure 3.

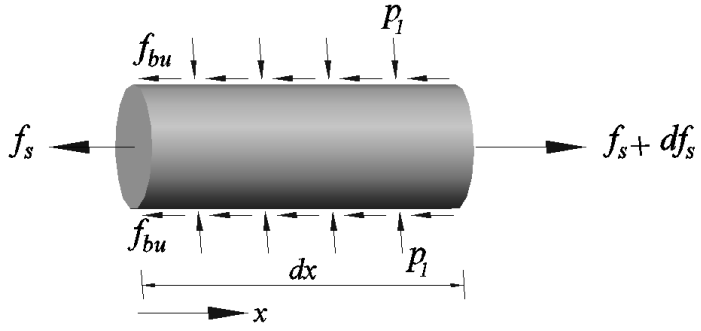

Figure 3: Stress on post-tensioning steel bar

The equilibrium for the forces acting on this element is shown below. To account for voids in grout, it is appropriate to deal with contact area by introducing a reduction factor of alpha (α) to maintain the contact area.

$$df_s*\pi r^2=f_{bu}*2\alpha\pi r*dx$$

$$dx=\frac{r}{2\alpha}\frac{1}{f_{bu}}df_s \quad (17)$$

where:

$$r=r_s+u_{r,s_1}=r_s+\frac{-p_1\left(1-\mu_s\right)}{E_s}r_s-\frac{\mu_s f_s}{E_s}r_s \quad (18)$$

The bond stress is also dependant on the normal stress which is exerted after the rupture as it describes by Coulomb's law of friction.

$$f_{bu}=\phi p_1 \quad (19)$$

Combining equation (18), (19) and (17) gives:

$$dx=\frac{1}{2\alpha\phi}\left(r_s+\frac{-p_1\left(1-\mu_s\right)}{E_s}r_s-\frac{\mu_s f_s}{E_s}r_s\right)\left(\frac{1}{p_1}\right)df_s$$

or

$$dx=\frac{r_s}{2\alpha\phi}\left(\frac{1}{p_1}+\frac{-\left(1-\mu_s\right)}{E_s}-\frac{1}{p_1}\frac{\mu_s f_s}{E_s}\right)df_s \quad (20)$$

Substitute (16) on (20) yields:

$$dx=\frac{r_s}{2\alpha\phi}\left(\frac{1}{\left(A+Bf_s\right)}-\frac{\left(1-\mu_s\right)}{E_s}-\frac{\mu_s f_s}{E_s}\frac{1}{\left(A+Bf_s\right)}\right)df_s$$

Integration of both sides yields:

$$\therefore\int_0^x dx=\int_0^{f_s}\frac{r_s}{2\alpha\phi}\left(\frac{1}{\left(A+Bf_s\right)}-\frac{\left(1-\mu_s\right)}{E_s}-\frac{\mu_s f_s}{E_s}\frac{1}{\left(A+Bf_s\right)}\right)df_s$$

or

$$x=\frac{r_s}{2\alpha\phi}\left[\left(\frac{1}{B}+\frac{\mu_s}{E_s}\frac{1}{B^2}\right)\ln\left(1+\frac{B}{A}f_s\right)-\left(\frac{1-\mu_s}{E_s}+\frac{\mu_s}{BE_s}\right)f_s\right] \quad (21)$$

Equation (21) estimates the re-anchorage length when the stress in the pre-stressing steel f_s is substituted by the effective pre-stress f_{se}. It is also gives the distribution of stress in the tendon along the re-anchorage length in post-tensioned concrete element.

Validation of this model will be carried in the following section against:

1) Finite Element model.
2) The UK Highway Agency BA51/95 model
3) Previous experimental data (Geddes and Soroka, 1964)

4 FINITE ELEMENT BOND MODELLING OF RUPTURED POST-TENSIONED TENDON

To model the re-anchoring of a ruptured tendon, the compatibility equation has to be solved at each interface between any two cylinders (for example m and n). The radial deformation at perimeter of cylinder m at interface it should equal the radial deformation at the perimeter of cylinder n, equation (22).

$$u_{r,m_i} = u_{r,n_i} \tag{22}$$

where: the radial deformation is a function of the applied normal and shear stresses are as shown below.

$$u_r = f\left(\sigma_r, \sigma_\theta, \sigma_z, \tau_{rz}, \tau_{r\theta}, \tau_{z\theta}\right) \tag{23}$$

In the longitudinal direction z, the slip s at a certain section is defined as the relative displacement between the two cylinders at the interface at that point.

$$\frac{ds}{dz} = \frac{df_m}{E_m} - \frac{df_n}{E_n}$$

or (24)

$$\frac{ds}{dz} = \varepsilon_m - \varepsilon_n$$

To solve these equations at each section along the tendon length, The ANSYS FE package was used. The problem was defined as an axi-symmetric model similar to the thick-wall cylinder. All of the materials (i.e. concrete, steel, grout, duct and end-plates) were modeled using 8-node elements with linear materials properties.

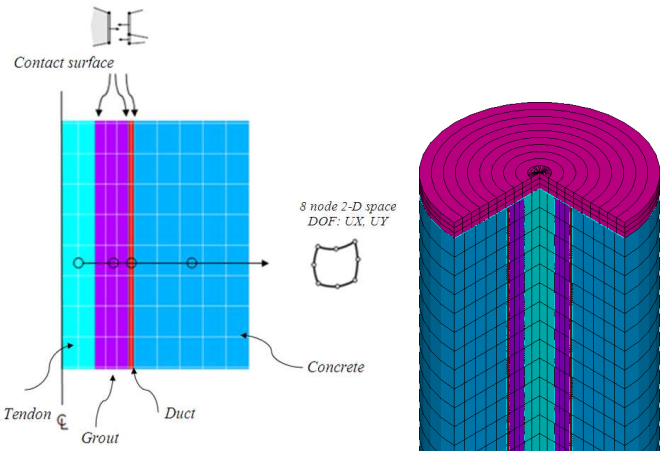

Figure 4: Details of axi-symmetric FE model

In this study, steel-grout, grout-duct, and duct-concrete interfaces were defined using surface-to-surface contact elements.

The contact between any two bodies occurs when the normal distance between two pairs of points on these bodies lies within specified tolerance. This normal distance is known as the penetration u_n, it depends on normal pressure p and contact stiffness k_n. When the normal distance is positive "gap", separation occurs and the contact pressure is set to zero. The normal contact behavior can be described in form of equation (25).

$$p = \begin{cases} 0 & \text{if } u_n > 0 \\ k_n u_n & \text{if } u_n \le 0 \end{cases} \tag{25}$$

The Coulomb friction law was used to model tangential behavior between steel and grout with zero cohesion as shown in equation (26). Other contact interfaces (i.e. grout-duct and duct concrete) were considered to be fully bonded. The slip takes place when the tangential deformation between two contact pairs exceeds the specified tolerance.

$$\tau = \phi p \tag{26}$$

The coefficient of friction Ø between grout and steel was found to be higher than the one between concrete and steel by 5% (Rabbat and Russell, 1985), thus the value of 0.42 is used for this model.

An augmented Lagrange multiplier algorithm and Penalty method were used to solve both the normal and tangential behaviors of the contact surface, respectively.

The post-tensioning stress was modeled by applying an initial stress in the steel elements in the model. The element birth and death technique within ANSYS's environment was used to deactivate and activate the elements composing the grout prior to applying pre-stresses and during the analysis, respectively to simulate the grouting process.

The modeling of rupture was carried out by introducing fully bonded surface-to-surface contact elements at the rupture location. The rupture of the tendon was then simulated by deactivating the contact elements.

A full Newton-Raphson solver with unsymmetric matrix storage was used to solve the model statically.

5 RESULTS AND DISCUSSION

The model results were compared with the experimental data given in the work of (Geddes and Soroka, 1964) and the DMRB - BA 51/95 model which is recommended by the Design Manual of Road and Bridges (Highway Agency, 1995) as shown in Figure 5.

Theoretical and experimental re-anchorage length was estimated at 95 percent of the average maximum strain (95% AMS) method (B.W. Russell and Burns, 1993)

For the same properties of the post-tensioned concrete beam which is described in (Geddes and Soroka, 1964), the axi-symmetric FE model predicted the re-anchorage length to be 1.45 m in com-

parison to the experimentally measured re-anchorage length of 0.99 m. On the other hand the theoretical model estimated the re-anchorage length to be 1.29 m. BA 51/95, however, has overestimated re-anchorage length by about 125% (i.e. 2.22 m) in comparison to experimental measurements and about 50% and 70% in comparison to the proposed FE and theoretical models, respectively.

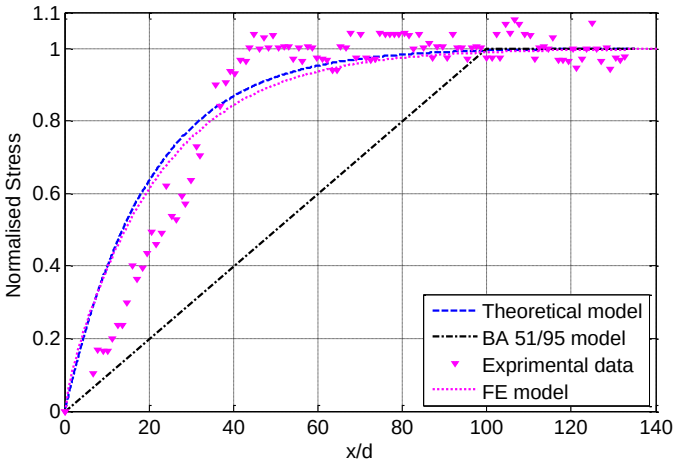

Figure 5: Tendon stress distribution over re-anchoring zone

The difference between theoretical and FE curves of stress distribution can be mainly attributed to the occurrence of slip, which is not considered in the theoretical model. See Figure 6.

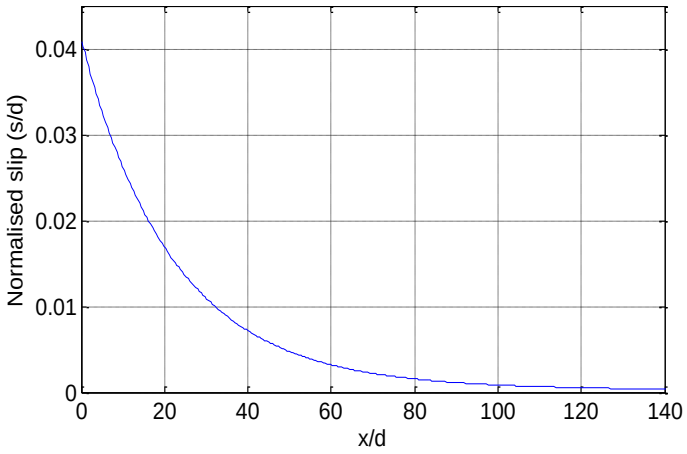

Figure 6: Slip at grout/steel interface

5.1 Non-linear behavior of grout

The circumferential stresses in the grout adjacent to the steel/grout interface were plotted in Figure 7. The results show that the circumferential stresses at the rupture location reach values exceeding the grout tensile strength. This indicates that cracks will be present in the radial direction in the grout; therefore the non-linear behavior of the grout needs to be considered to simulate the re-anchorage phenomenon correctly.

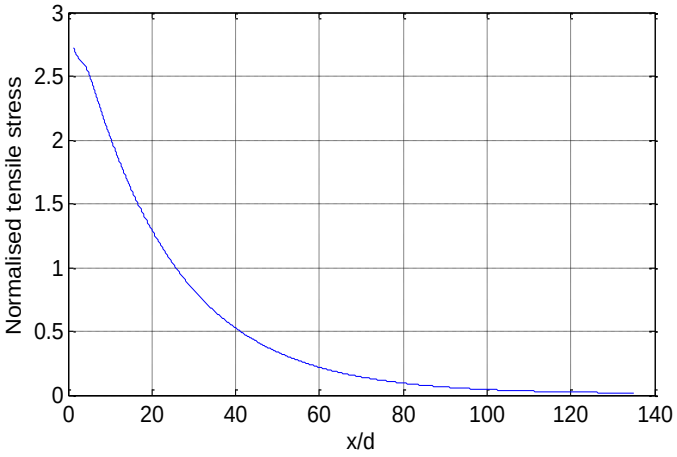

Figure 7: Circumferential stresses in grout

One of the disadvantages of the axi-symmetric model, is that, the number of radial cracks has to be assumed in order to account for the non-linear behavior of concrete (Lundgren, 2005, Ruiz et al., 2007) . This phenomenon can be conveniently modeled using 3D finite element analysis to account for the non-linear materials behavior as well as the different geometric shapes.

6 CONCLUSION

The development of linear numerical models to estimate the transfer of pre-stress force from a ruptured tendon into the surrounding materials had been described in this paper. The model employs the linear elastic theory of thick-wall cylinders to account for equilibrium of forces and compatibility of displacements at the confining materials interfaces (i.e. concrete, duct and grout). The models consider the effect of axial stresses in the tendon and confining materials as well as the bond behavior at interfaces.

Comparisons between the proposed model, FE model, UK Highway Agency BA51/95 model and previous experimental data show the ability of the proposed model to estimate the re-anchorage length and stress distribution along the ruptured bonded post-tensioning tendon.

It is proposed to improve the model to consider nonlinear behavior of materials, geometrical aspects, ordinary reinforcement and behavior in 3D. A model accounts for such factors helps in assessing the post-tensioned concrete elements with ruptured tendon.

7 REFERENCES

B.W. RUSSELL & BURNS, N. H. (1993) Design Guidelines for Transfer, Development and Debonding of Large Diameter Seven Wire Strands in Pretensioned Concrete Girders. Research Report 1210-5F. Austin, Texas, Center for Transportation Research, the University of Texas at Austin.

BELHADJ, A. & BAHAI, H. (2001) Friction-slip: an efficient energy dissipating mechanism for suddenly released prestressing bars. Engineering Structures, 23**,** 934-944.

BS 5400 - 4 (1990) Steel, concrete and composite bridges. Code of practice for design of concrete bridges, London, B.S.I.

BUCHNER, S. H. & LINDSELL, P. (1987) Testing of Prestressed Concrete Structures During Demolition. Structural assessment : the use of full and large scale testing. London ; Boston, Butterworths.

BUCHNER, S. H. & LINDSELL, P. (1988) Controlled Demolition of Prestressed Concrete Structures. IN Y. KASAI (Ed.) Demolition and reuse of concrete and masonry: Second International RILEM Symposium.

CAVELL, D. G. & WALDRON, P. (2001) A residual strength model for deteriorating post-tensioned concrete bridges. Computers & Structures, 79**,** 361-373.

CEB-FIP MC90 (1990) CEB-FIP model code 1990 (Design Code), Telford Thomas.

CONCRETE SOCIETY (2002) Durable bonded post-tensioned concrete bridges. Technical Report Technical Report 47 (TR47). 2nd ed.

CORONELLI, D., CASTEL, A., VU, N. A. & FRANÇOIS, R. (2009) Corroded post-tensioned beams with bonded tendons and wire failure. Engineering Structures, 31**,** 1687-1697.

GEDDES, J. D. & SOROKA, I. (1963) Effect of grout properties on structural behaviour of post-tensioned concrete beams. Magazine of Concrete Research. London, Thomas Telford

GEDDES, J. D. & SOROKA, I. (1964) Effect of grout properties on transmission length in grout-bonded post-tensioned concrete beams. Magazine of Concrete Research. London, Thomas Telford

GILBERT, R. I. & MICKLEBOROUGH, N. C. (1990) Design of prestressed concrete, London, E & FN Spon.

GREAT BRITAIN HIGHWAYS AGENCY, FRANCE SERVICE D'ÉTUDES TECHNIQUES DES ROUTES ET, A., TRANSPORT RESEARCH LABORATORY & LABORATOIRE CENTRAL DES PONTS ET CHAUSSÉES (1999) Post-tensioned concrete bridges : Anglo-French liaison report, London, Thomas Telford.

HIGHWAY AGENCY (1995) The assessment of Concrete Structures affected by Steel Corrosion. IN AGENCY, T. H. (Ed.) BA51/95: Design Manual for Roads and Bridges DMRB, vol.3, Section 4, Part 13

JANNEY, J. R. (1954) Nature of bond in pre-tensioned prestressed concrete. American Concrete Institute Journal, 26**,** 736-1.

JEYASEHAR, C. A. & SUMANGALA, K. (2006) Damage assessment of prestressed concrete beams using artificial neural network (ANN) approach. Computers & Structures, 84**,** 1709-1718.

LUNDGREN, K. (2005) Bond between ribbed bars and concrete. Part 1: Modified model. Magazine of Concrete Research, 57**,** 371-382.

LUTHI, T., DIEPHUIS, J. R., A, J. J. I., BREEN, J. E. & KREGER, M. E. (2008) Effects of Duct Types and Emulsifiable Oils on Bond and Friction Losses in Posttensioned Concrete. Journal of Bridge Engineering, 13**,** 100-109.

MARTI, P., ULLNER, R., FALLER, M., CZADERSKI, C. & MOTAVALLI, M. (2008) Temporary corrosion protection and bond of prestressing steel. ACI Structural Journal-American Concrete Institute, 105**,** 51-59.

NCHRP (1998) Durability of Precast Segmental Bridges: Final Report. NCHRP Web Doc 15

RABBAT, B. G. & RUSSELL, H. G. (1985) Friction Coefficient of Steel on Concrete or Grout. Journal of Structural Engineering, 111**,** 505-515.

RUIZ, M. F., MUTTONI, A. & GAMBAROVA, P. G. (2007) A RE-EVALUATION OF TEST RESULTS ON BOND IN R/C BY MEANS OF FE MODELING. Studies and Reseaches, Politecnico di Milano, Italy, 27.

SCHUPACK, M. & JOHNSTON, D. W. (1974) Bond Development Length Tests of A Grouted 54 Strand Post-Tensioning Tendon

Journal of The American Concrete Institute, 71**,** 522-525.

TIMOSHENKO, S. P. (1976) Strength of materials, Huntington, N.Y., Robert E. Krieger Pub. Co.

WATANABE, K., TADOKORO, T. & TANIMURA, Y. (2011) Evaluation for Flexural-load Capacity of Prestressed Concrete Girders with Broken Tendons. Quarterly Report of RTRI, 52**,** 224-229.

WOODWARD, R. J. & WILLIAMS, F. W. (1989) Collapse of Ynys-Y-Gwas Bridge, West-Glamorgan - Discussion. Proceedings of the Institution of Civil Engineers Part 1-Design and Construction, 86**,** 1177-1191.

ZENG, Y. H., HUANG, Q. H., GU, X. L. & ZHANG, W. P. (2010) Experimental Study on Bending Behavior of Corroded Post-Tensioned Concrete Beams. 41096 ed. Honolulu, HI, ASCE.

NOTATION

A_s: Cross sectional area of pre-stressing bar

A_g: Cross sectional area of grout

A_d: Cross sectional area of duct

A_c: Cross sectional area of concrete

a: Internal diameter of cylinder

b: External diameter of cylinder

D: Nominal diameter of tendon (mm)

f_{ci}: Concrete strength at transfer (N/mm^2)

f_s : Longitudinal stress in pre-stress steel bar at a section

f_g: Longitudinal stress in grout at a section

f_d: Longitudinal stress in duct at a section

f_c: Longitudinal stress in concrete at a section

E: Young's modulus of cylinder material

E_s: Young's modulus of pre-stressing bar

E_g: Young's modulus of grout

E_d: Young's modulus of duct

$E_{concrete}$: Young's modulus of concrete

k_t: Coefficient depends on type of tendon, it equals 600 for bars

l_t: Transfer length

p_i: Applied internal pressure in the radial direction

p_e: Applied external pressure in the radial direction

p_1: Exerted pressure at interface 1

p_2: Exerted pressure at interface 2

p_3: Exerted pressure at interface 3

r_s: Nominal radius of pre-stressing steel bar

r_{g1}: Radius of grout cylinder at interface 1r_{g2}: Radius of grout cylinder at interface 2

r_{d2}: Radius of the duct at interface 2 (Internal radius)

r_{d3}: Radius of the duct at interface 3 (External radius)

r_{c3}: Radius of the concrete cylinder at interface 3

r_{c4}: Measured radius of the concrete cylinder to the nearest concrete surface

S: Number of strands

s: Slip

u_r: Radial deformation at radius equal r

μ: Poisson's ratio of cylinder material

$u_{r,s1}$: Radial deformation of pre-stressing bar at interface 1

$u_{r,g1}$: Radial deformation of grout cylinder at interface 1

$u_{r,g2}$: Radial deformation of grout cylinder at interface 2

$u_{r,d2}$: Radial deformation of the duct at interface 2

$u_{r,d3}$: Radial deformation of duct cylinder at interface 3

$u_{r,c3}$: Radial deformation of the concrete cylinder at interface 3

σ_z: Applied stress in the longitudinal direction Z

Ø: Coefficient of friction

τ: Tangential shear stress

μ: Poisson's ratio of cylinder material

μ_s: Poisson's ratio of pre-stressing bar

μ_g: Poisson's ratio of grout

μ_d: Poisson's ratio of duct

μ_c: Poisson's ratio of duct

APPENDIX

$$C_1 = -\frac{r_s(1-\mu_s)}{E_s} - \frac{r_{g_1}^{\,3}(1-\mu_g)}{E_g\left(r_{g_2}^{\,2}-r_{g_1}^{\,2}\right)} - \frac{r_{g_1} r_{g_2}^{\,2}(1+\mu_g)}{E_g\left(r_{g_2}^{\,2}-r_{g_1}^{\,2}\right)}$$

$$C_2 = \frac{2 r_{g_1} r_{g_2}^{\,2}}{E_g\left(r_{g_2}^{\,2}-r_{g_1}^{\,2}\right)}$$

$$C_3 = 0$$

$$C_4 = \frac{2 r_{g_1}^{\,2} r_{g_2}}{E_g\left(r_{g_2}^{\,2}-r_{g_1}^{\,2}\right)}$$

$$C_5 = -\frac{r_{d_2}\left(r_{d_3}^{\,2}(1+\mu_d)+r_{d_2}^{\,2}(1-\mu_d)\right)}{E_d\left(r_{d_3}^{\,2}-r_{d_2}^{\,2}\right)} - \frac{r_{g_2}\left(r_{g_2}^{\,2}(1-\mu_g)+r_{g_1}^{\,2}(1+\mu_g)\right)}{E_g\left(r_{g_2}^{\,2}-r_{g_1}^{\,2}\right)}$$

$$C_6 = \frac{2 r_{d_2} r_{d_3}^{\,2}}{E_d\left(r_{d_3}^{\,2}-r_{d_2}^{\,2}\right)}$$

$$C_7 = 0$$

$$C_8 = \frac{2 r_{d_2} r_{d_3}^{\,2}}{E_d\left(r_{d_3}^{\,2}-r_{d_2}^{\,2}\right)}$$

$$C_9 = -\frac{r_{d_3}\left(r_{d_2}^{\,2}(1+\mu_d)+r_{d_3}^{\,2}(1-\mu_d)\right)}{E_d\left(r_{d_3}^{\,2}-r_{d_2}^{\,2}\right)} - \frac{r_{c_3}\left(r_{c_3}^{\,2}(1-\mu_c)+r_{c_4}^{\,2}(1+\mu_c)\right)}{E_c\left(r_{c_4}^{\,2}-r_{c_3}^{\,2}\right)}$$

$$k_1 = r_s - r_{g_1} - \frac{f_s \mu_s r_s}{E_s} - \frac{A_s f_s \mu_g r_{g_1}}{A_b E_g}$$

$$k_2 = r_{g_2} - r_{d_2} + \frac{A_s f_s \mu_g r_{g_2}}{A_b E_g} - \frac{A_s f_s \mu_d r_{d_2}}{A_b E_d}$$

$$k_3 = r_{d_3} - r_{c_3} - \frac{A_s f_s \mu_c r_{c_3}}{A_b E_c} + \frac{A_s f_s \mu_d r_{d_3}}{A_b E_d}$$